




Shensong Yangxin Capsule Reduces the Susceptibility of Arrhythmia in db/db Mice via Inhibiting the Inflammatory Response Induced by Endothelium Dysfunction

Jiehan Zhang ^{1,2}, Hongrong Li^{3,4}, Dandong Wang^{1,2}, Jiaojiao Gu^{2,5}, Yunlong Hou ^{1,2}, Yiling Wu ^{1,2}

¹Hebei Medical University, Shijiazhuang, People's Republic of China; ²National Key Laboratory of Collateral Disease Research and Innovative Chinese Medicine, Shijiazhuang, People's Republic of China; ³Key Laboratory of State Administration of TCM (Cardio-Cerebral Vessel Collateral Disease), Shijiazhuang, People's Republic of China; ⁴Hebei Yiling Hospital, Shijiazhuang, People's Republic of China; ⁵Hebei University of Traditional Chinese Medicine, Shijiazhuang, People's Republic of China

Correspondence: Yiling Wu; Yunlong Hou, Hebei Medical University, Shijiazhuang, People's Republic of China, Email professorylw@163.com; hounlonghrb@hotmail.com

Purpose: The aim of our study was to investigate the mechanism by which the Chinese compound Shensong Yangxin Capsule (SSYX) reduces susceptibility to arrhythmia in db/db mice.

Methods: The db/db mice without drug treatment served as the model group. Other-treated db/db mice were administered SSYX for 8 weeks. Electrocardiogram (ECG), electrical mapping, pathological changes, immunofluorescence staining, real-time quantitative PCR, and Western blot analyses were then conducted.

Results: SSYX decreased arrhythmia susceptibility and shortened the abnormal ECG parameters of db/db mice. Meanwhile, SSYX restored irregular conduction direction and shortened the conduction time of the isolated heart. HE and Masson staining showed that SSYX alleviated inflammatory infiltration and collagen fiber deposition. Western blot showed that SSYX decreased the protein expression of ICAM-1, VCAM-1, and MCP-1 and increased the protein expression of occludin, ZO-1, eNOS, and Cx43. SSYX also increased the content of NO, decreased ET-1, TNF- α , IL-1 β , IL-6, MCP-1, and CCR-2 mRNA expression, and increased Kv 4.2, Kv 4.3, Cav 1.2, and Nav 1.5 mRNA expression. Furthermore, SSYX decreased the fluorescence intensity of F4/80 and iNOS, increased the fluorescence intensity of CD31 and eNOS, and improved the Cx43 and α -actinin connection structure in cardiac tissues. The above therapeutic effects of SSYX were inhibited by L-NAME.

Conclusion: SSYX reduced the susceptibility of db/db mice to arrhythmia by inhibiting the inflammatory response and macrophage polarization, and this effect of SSYX occurred through protection of endothelial cell function.

Keywords: arrhythmia, endothelial cell function, inflammation, macrophage

Introduction

Cardiovascular events are often characterized by arrhythmia, and arrhythmia is also a complication of organic heart diseases, including coronary heart disease,¹ myocardial infarction,² and heart failure.³ According to previous studies, electrical and structural remodeling of the heart and reentrant circuit formation are the basic mechanisms of arrhythmia triggering and maintenance.⁴⁻⁶ Recently, myocardial microcirculation dysfunction in arrhythmia has gained attention due to its direct effect on endothelial cells. Experiments and clinical studies have demonstrated that endothelial dysfunction is associated with arrhythmia and increased vascular inflammation.^{7,8}

Previous studies have shown that inflammation plays a role in arrhythmias.⁹ Cardiomyocyte health and extracellular matrix composition can be affected by macrophages in the heart.¹⁰ Additionally, cardiomyocytes and macrophages interact through connexin 43, which assists in electrical coupling.¹¹ The coculture of macrophages and cardiomyocytes

demonstrated that macrophage phenotype and gap junction status may influence cardiomyocyte action potential duration (APD), possibly contributing to arrhythmia.¹² Thus, methods of reducing inflammation can be used to treat arrhythmia.

According to clinical studies, diabetes has been identified as an independent risk factor for atrial fibrillation and sudden cardiac death.^{13,14} However, there is no specific conclusion on the mechanism that predisposes diabetes patients to arrhythmia or a treatment plan to reduce this susceptibility. Diabetes mellitus is characterized by low-grade chronic inflammation.¹⁵ By releasing proinflammatory cytokines, macrophages contribute to the progression of diabetes.¹⁶ Diabetes mellitus also causes endothelial dysfunction, which contributes to diabetic vascular complications.¹⁷ Therefore, we suppose that the increased arrhythmia susceptibility in diabetic patients may be a result of the inflammatory response mediated by endothelial dysfunction.

Shensong Yangxin (SSYX) capsules are an antiarrhythmic Chinese patent medicine that can improve microcirculation, protect endothelial cells, and reverse myocardial structural remodeling, electrical remodeling, and neural remodeling after myocardial infarction.^{18–23} SSYX has been widely used to treat various arrhythmias by regulating multiple ion and non-ion channels.^{24–26} However, whether SSYX can reduce arrhythmia susceptibility in patients with diabetes has not been studied. Therefore, we selected leptin receptor-deficient mice, a typical animal model of type 2 diabetes, to determine whether SSYX reduces the arrhythmia susceptibility and its corresponding mechanism.

Materials and Methods

Animal Models and Drugs

Experiments were performed using male leptin receptor-deficient db/db mice (C57BL/KS-lepr^{db}/lepr^{db}), and db/m mice aged 4–5 weeks served as controls. Animals were purchased from the Changzhou Kawensi laboratory and housed in the animal barrier environment of the New Drug Evaluation Center of Shijiazhuang Yiling Pharmaceutical Academician Workstation Research Institute. The environmental temperature and humidity were suitable, the daily light/dark cycle was 12/12 hours, and all mice had free access to water and food for 1 week. Then, db/db mice were randomly assigned to four groups consisting of 10 mice each, including the model group, SSYX low-dose group (SSYX-L), SSYX high-dose group (SSYX-H), and SSYX high-dose add N G-Nitro-L-arginine Methyl Ester, Hydrochloride (L-NAME) group (L-SSYX-H). The SSYX-L group and SSYX-H group were given 0.4 g/kg/d and 1.6 g/kg/d SSYX respectively. The L-SSYX-H group freely ingested animal drinking water containing L-NAME while given high-dose SSYX. The control group and model group were given the corresponding amount of CMC-Na according to their weights. Each group was perfused once a day for 8 weeks. All animal experiments were approved by the new drug evaluation center of Hebei Yiling Pharmaceutical Research Institute Co., Ltd (No. 2021060) and were in accordance with the National Institutes guidelines for the Care and Use of Laboratory Animals.

Blood Glucose and Body Weight Measurement

Blood glucose was measured by cutting the tail approximately 1 mm to make the vein blood flow out naturally and then discarding the first drop of blood. Blood glucose levels were assessed using a OneTouch Ultra Easy glucose monitoring system and test strips. Blood glucose and body weight were measured once a week.

Arrhythmia Induced by Intraperitoneal Injection of Isoproterenol

After the last intragastric administration, six mice in each group were fasted with free access to water for 12 hours and intraperitoneally injected with pentobarbital sodium anesthesia. When mice were unresponsive to physical stimuli, they were fixed in the supine position. The surface electrocardiogram (ECG) was recorded (LabChart 8, ADInstruments, Australia) using subcutaneous needle electrodes attached to mouse limbs. A Powerlab physiological recorder was used to collect and analyze the ECG parameters of the mice. After the ECG waveform was running stably, isoproterenol was intraperitoneally injected, and then the arrhythmia induction rate and parameter changes in each group were calculated.

Langendorff Heart Preparation and Electrophysiological Studies

Three mice in each group were intraperitoneally injected with heparin sodium (3125 U/kg) and anesthetized by intraperitoneal injection of 2% pentobarbital sodium (50 mg/kg) 15 minutes later. The mice were fixed on the experimental platform, and the chest skin was cut open to expose the xiphoid process. Then, the chest was cut open along the middle of the left and right costal arches on both sides of the xiphoid process to expose the heart. The heart was lifted with tweezers, quickly cut off along the rear of the lung, and then placed in precooled oxygen-containing (95% O₂ + 5% CO₂) Krebs–Henseleit (KH) perfusion solution (KH perfusion fluid composition (mM): 119 NaCl, 25 NaHCO₃, 4 KCl, 1.2 KH₂PO₄, 1 MgCl₂, 1.8 CaCl₂ 2H₂O, and 10 D-glucose). The ventricle was gently pressed with tweezers to discharge blood from the aorta to determine the broken end of the aortic root, and then the surrounding excess tissue was cut off. The Langendorff perfusion system was started in advance, and the temperature of the perfusion fluid was set to 37 °C. Then, the perfusion speed was adjusted to 2 mL/min, and the whole perfusion system was filled with KH perfusion fluid. After preparing for perfusion, the perfusion needle was connected to the system, tweezers were used to support the broken end of the aorta, quickly connected to the perfusion needle, and fixed for retrograde perfusion, pumping residual blood out of the heart and maintaining beating. Two sets of silver bipolar electrodes coated with Teflon were placed on the appendages of the right atrium and the left ventricle. Then, the MappingLab matrix multichannel electrophysiological mapping system (Electrical Mappinglab 64, England) was used to record signals.

HE and Masson Trichrome Staining

Histopathological examination of myocardial tissues was performed with HE and Masson trichrome staining. The heart samples were fixed in 4% paraformaldehyde solution for 24 h, embedded in paraffin and cut into slices of 4 µm. After deparaffinization, tissue sections were stained with HE and Masson's trichrome. The slices were observed under a light microscope (Leica Microsystems, Wetzlar, Germany).

Immunofluorescence Double Staining

Heart tissues were sliced into 4 µm sections, which were then paraffin embedded. After conventional dewaxing to water, the sections underwent microwave heat repair with EDTA sodium citrate antigen repair solution. After incubation with 3% hydrogen peroxide solution at 37 °C in the dark for 10 minutes, the sections were washed with PBS and incubated with 5% BSA at room temperature for 30 minutes. The tissues were incubated with antibodies against CD31 (Abcam, ab281583, 1:500 dilution, UK) and endothelial nitric oxide synthase (eNOS) (Servicebio, GB12086, 1:500 dilution, China) overnight at 4 °C. After being washed with PBS, the tissues were incubated with Alexa Fluor 488 (Servicebio, GB25303, 1:500 dilution, China) and coralite594 (Proteintech, SA00013-3-100, 1:300 dilution, China) for 1 h at room temperature. Images were captured with an inverted laser confocal microscope (ZEISS, LSM710, Germany).

Tyramide Signal Amplification (TSA)

We selected a TSA-compatible double-color immunostaining protocol using primary antibodies from the same host species. Microwave heat repair and incubation with 3% hydrogen peroxide solution were the same as before. Sections were blocked with 3% BSA for 30 minutes and then incubated with F4/80 (Servicebio, GB113373, 1:400 dilution, China) and inducible nitric oxide synthase (iNOS) (Servicebio, GB11119, 1:500 dilution, China) to evaluate macrophage polarization. Other sections were incubated with connexin 43 (Cx43) (Proteintech, 26980-1-AP, 1:300 dilution, China) and α -actinin (Servicebio, GB111556, 1:500 dilution, China) to assess cardiomyocyte gap junctions. The tissues were incubated with TSA-FITC and TSA-CY3 separately and labeled green and red, respectively. Images were captured with an inverted laser confocal microscope (ZEISS, LSM710, Germany).

Enzyme-Linked Immunosorbent Assay (ELISA)

The myocardial tissue level of nitric oxide (NO) was examined with an ELISA kit. After thoroughly grinding the tissue, the homogenate was extracted by centrifugation at 3000×g at 4 °C for 15 min. The level of NO was detected according to the kit instructions.

Real-Time Quantitative PCR

Total RNA from the hearts was extracted using TRIzol (Solarbio, R1100, China). Conversion to cDNA was performed using SweScript All-in-One First-Strand cDNA Synthesis SuperMix for qPCR (Servicebio, G3337-100, China), and 2×Universal Blue SYBR Green qPCR Master Mix (Servicebio, G3326-05, China) was used to accomplish DNA template amplification. Transcript analysis of genes encoding tumor necrosis factor- α (TNF- α), interleukin-1 β (IL-1 β), endothelin-1 (ET-1), Kv 4.2, Kv 4.3, Cav 1.2, Nav 1.5, interleukin-6 (IL-6), monocyte chemotactic protein-1 (MCP-1), chemokine receptor 2 (CCR-2), and glyceraldehyde 3-phosphate dehydrogenase (GAPDH) was carried out using quantitative real-time PCR on an Applied Biosystems 7900HT Fast Real-Time PCR System. The primers were from Servicebio, and their sequences are provided in Table 1. Transcript data were normalized to the arithmetic mean of GAPDH and analyzed using the threshold cycle (C_T) relative quantification method. The mRNA expression levels were quantified using the $2^{-\Delta\Delta C_T}$ method for comparison. The PCR conditions consisted of an initial denaturing step at 95 °C for 30s, followed by 40 cycles of 95 °C for 15s and an annealing step at 60 °C for 30s.

Western Blot Analysis

Protein extraction from cardiac tissue was performed using RIPA lysis buffer (Seven Biotech, SW104-01, China). The protein concentration was determined by BCA assay (Seven Biotech, SW101-02, China). Sample proteins were then separated by Easy PAGE GeL Bis-Tris, 4~20% (Seven Biotech, SW160-12, China) before transferring to a 0.45 μ m polyvinylidene fluoride (PVDF) membrane (Millipore, America). Immunoblots were blocked with Rapid Blocking

Table 1 Primers for Real-Time PCR

| Gene | Primer Sequence (5' to 3') | bp |
|---------------|---|-----|
| GAPDH | Forward: CCTCGTCCCGTAGACAAAATG Reverse: TGAGGTCAATGAAGGGGTCGT | 133 |
| TNF- α | Forward: CCCTCACACTCACAACCACC Reverse: CTTTGAGATCCATGCCGTTG | 93 |
| IL-1 β | Forward: GCATCCAGCTTCAAATCTCGC Reverse: TGTTTCATCTCGGAGCCTGTAGTG | 256 |
| ET-1 | Forward: GCCACAGACCAGGCAGTTAGAT Reverse: TCCAACCTTCGTAGTTTCCTTCC | 206 |
| Kv 4.2 | Forward: AAGTTGCCACCGTCAATCG Reverse: TCGGCTGTTGGATAGTGGAGTT | 206 |
| Kv 4.3 | Forward: CAGTCGCTCCAGCCTTAATTTG Reverse: GACGACATTGCTGGTTATGGAAG | 187 |
| Nav 1.5 | Forward: ATCGTGCTGAATAAGGGCAAAC Reverse: CCATGAACACACAGTTGGTTAGGAT | 166 |
| Cav 1.2 | Forward: TGTCTGACCCTGAAGAACCCTATC Reverse: CAACCATTGCGGAGGTAAGC | 269 |
| IL-6 | Forward: CTGCAAGAGACTTCCATCCAG Reverse: AGTGGTATAGACAGGTCTGTTGG | 131 |
| MCP-1 | Forward: TAAAAACCTGGATCGGAACCAAA Reverse: GCATTAGCTTCAGATTTACGGGT | 120 |
| CCR-2 | Forward: ATCCACGGCATACTATCAACATC Reverse: TCGTAGTCATACGGTGTGGTG | 89 |

Abbreviations: GAPDH, glyceraldehyde 3-phosphate dehydrogenase; TNF- α , tumor necrosis factor- α ; IL-1 β , Interleukin-1 β ; ET-1, endothelin-1; IL-6, Interleukin-6; MCP-1, monocyte chemotactic protein-1; CCR-2, chemokine receptor 2.

Buffer (Seven Biotech, SW162-02, China). Then, the blots were incubated overnight at 4 °C with primary antibodies against Zonula occludens-1 (ZO-1) (Proteintech, 21773-1-AP, 1:3000 dilution, China), occludin (Proteintech, 66378-1-Ig, 1:2000 dilution, China), intercellular cell adhesion molecule-1 (ICAM-1) (Abcam, ab282575, 1:1000 dilution, UK), vascular cell adhesion molecule-1 (VCAM-1) (Abcam, ab134047, 1:1000 dilution, UK), Cx43 (Proteintech, 26980-1-AP, 1:2000 dilution, China), eNOS (Servicebio, GB11086, 1:500 dilution, China), MCP-1 (Proteintech, 66272-1-Ig, 1:2000 dilution, China), and GAPDH (Servicebio, GB15004, 1:1000 dilution, China). After washing with TBST, specific secondary antibodies were applied for 1 h at room temperature. The blots were again washed sequentially in TBST before imaging on the Odyssey CLX Imager Dual-color infrared imaging (LI-COR) system. The amount of protein on the immunoblots was quantified using ImageJ software, and the expression level of each protein was normalized to that of GAPDH.

Statistical Analysis

All statistical analyses were performed using SPSS version 26.0 software. Arrhythmia inducibility was analyzed using Fisher's exact test. Comparisons between groups were performed with ANOVA, and the least significant difference method was used for post hoc multiple comparisons. Data are expressed as the mean \pm SD. A P value < 0.05 was considered statistically significant.

Results

Changes in Weight and Blood Glucose

As shown in Figure 1, body weight and blood glucose were higher in db/db mice, and they did not change significantly after treatment with SSYX ($P < 0.05$).

SSYX Reduced Arrhythmia Susceptibility in db/db Mice

Intraperitoneal injection of isoproterenol was used to assess arrhythmia susceptibility in each group. As shown in Figure 2, the model group was highly susceptible to induced arrhythmia in comparison to the control group and showed typical arrhythmic electrocardiogram expressions. SSYX reduced the arrhythmia susceptibility of db/db mice. However, the effect of SSYX was antagonized by L-NAME.

ECG Parameters at Baseline and After Intraperitoneal Injection of Isoproterenol

As shown in Figure 3, the PR interval, RR interval, P-wave duration, QT interval, and QTc duration were prolonged in the model group in comparison to the control group ($P < 0.05$ or $P < 0.01$). Compared with the model group, the above parameters were shortened in the SSYX-L and SSYX-H groups ($P < 0.05$ or $P < 0.01$).

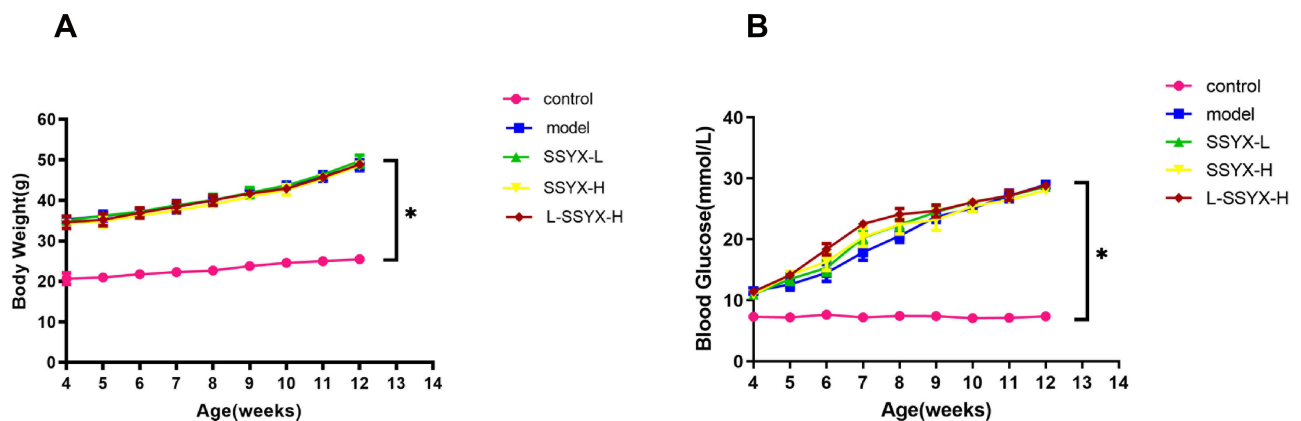


Figure 1 Body weight and blood glucose in each group. (A) Db/db mice put on body weight. (B) Db/db mice have elevated blood glucose. Values measured are presented as the mean \pm SD ($n = 10$). * $P < 0.05$ vs control group.

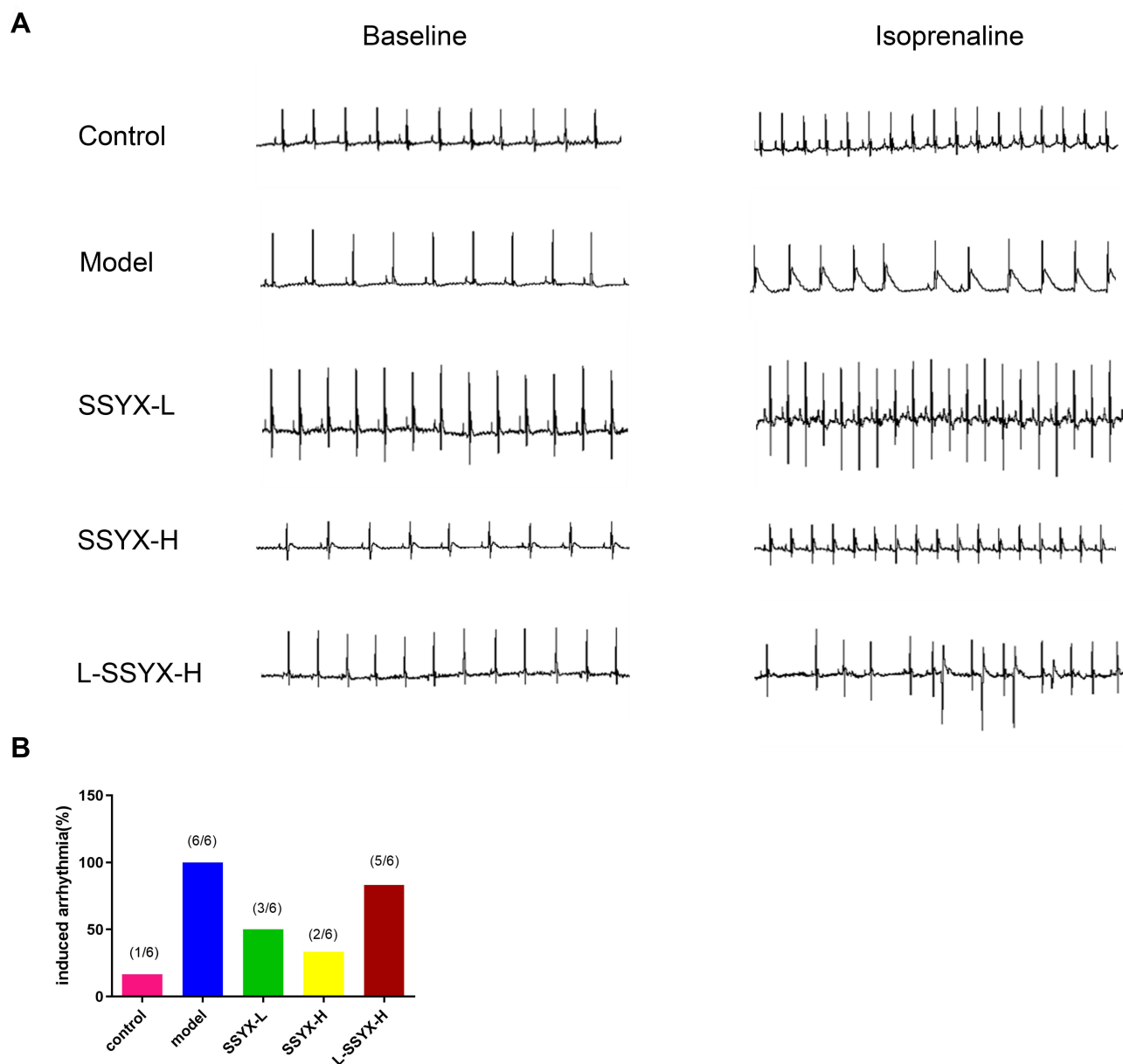


Figure 2 Typical electrocardiogram expressions before and after intraperitoneal isoprenaline and arrhythmia susceptibility in each group. **(A)** Typical electrocardiogram expressions before and after intraperitoneal isoprenaline in each group. **(B)** Arrhythmia induction rate in each group ($n = 6$).

As shown in Figure 4, the heart rate in each group increased after the intraperitoneal injection of isoproterenol. Compared with the control group, the PR interval, RR interval, P-wave duration, QT interval, and QTc interval were prolonged in the model group ($P < 0.05$ or $P < 0.01$). Compared with the model group, the above parameters were shortened in the SSYX-H group ($P < 0.05$ or $P < 0.01$).

Electrophysiological Changes in Isolated Hearts

Figure 5 illustrates the conduction direction and time in the atrium and ventricle. The model group and the L-SSYX-H group showed irregular conduction direction and prolonged conduction time ($P < 0.01$). The SSYX-H group showed a regular conduction direction and shortened conduction time compared to the model group and the L-SSYX-H group ($P < 0.01$).

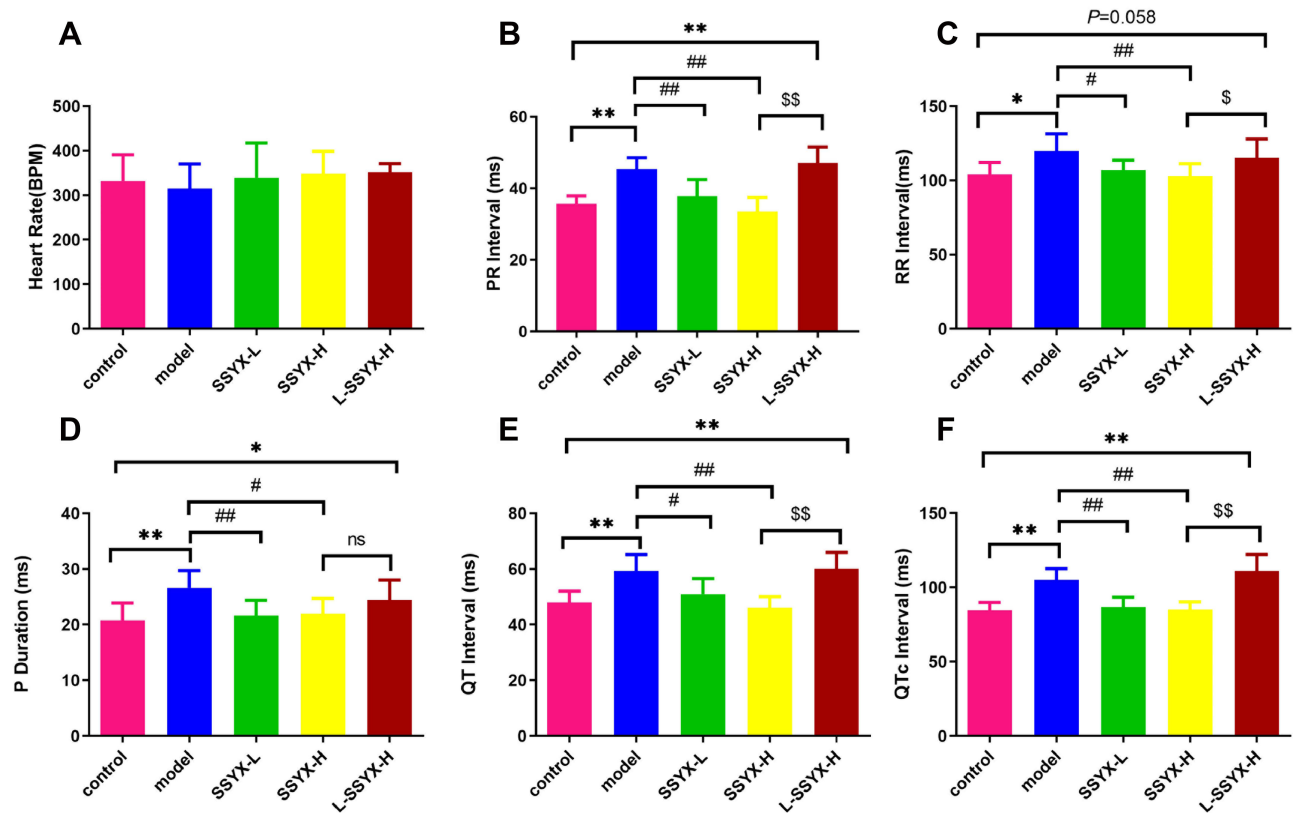


Figure 3 ECG parameters at baseline in each group. (A) The heart rate, (B) PR interval, (C) RR interval, (D) P duration, (E) QT interval, and (F) QTc interval in each group. Values measured are presented as the mean \pm SD ($n = 6$). ** $P < 0.01$ vs control group. * $P < 0.05$ vs control group. ### $P < 0.01$ vs model group. ## $P < 0.05$ vs model group. \$\$ $P < 0.01$ vs SSYX-H group. \$ $P < 0.05$ vs SSYX-H group.

Abbreviations: n.s., no statistical significance.

SSYX Administration Affects the Ion Channel mRNA Expression

As shown in Figure 6, Kv 4.2, Kv 4.3, Cav 1.2, and Nav 1.5 mRNA expression levels were reduced in the model group and the L-SSYX-H group compared with those in the control group ($P < 0.05$ or $P < 0.01$). Compared with the model group, Kv 4.2, Kv 4.3, Cav 1.2, and Nav 1.5 mRNA expression levels were upregulated in the SSYX-H group ($P < 0.05$ or $P < 0.01$).

SSYX Improved the Gap Junction of Myocardial Cells and Upregulated the Protein Expression of Cx43

As shown in Figure 7A, the Cx43 and α -actinin connection structure was chaotic in the model group and L-SSYX-H group, while in the SSYX-L group and the SSYX-H group, it was clear, and Cx43 was located around α -actinin. As shown in Figure 7B, the protein expression of Cx43 was reduced in the model group and the L-SSYX-H group compared with the control group ($P < 0.05$ or $P < 0.01$). Compared with that in the model group, the protein expression of Cx43 was upregulated in the SSYX-L group and the SSYX-H group ($P < 0.01$). Compared with that in the SSYX-H group, the protein expression of Cx43 was reduced in the L-SSYX-H group ($P < 0.01$).

SSYX Improved the Cardiac Tissue Inflammatory Response and Collagen Fiber Deposition

As shown in Figure 8A, the results of HE staining showed a typical myofibrillar structure in the control group, while the model group and the L-SSYX-H group showed infiltration of inflammatory cells and some cardiomyocytes with swelling

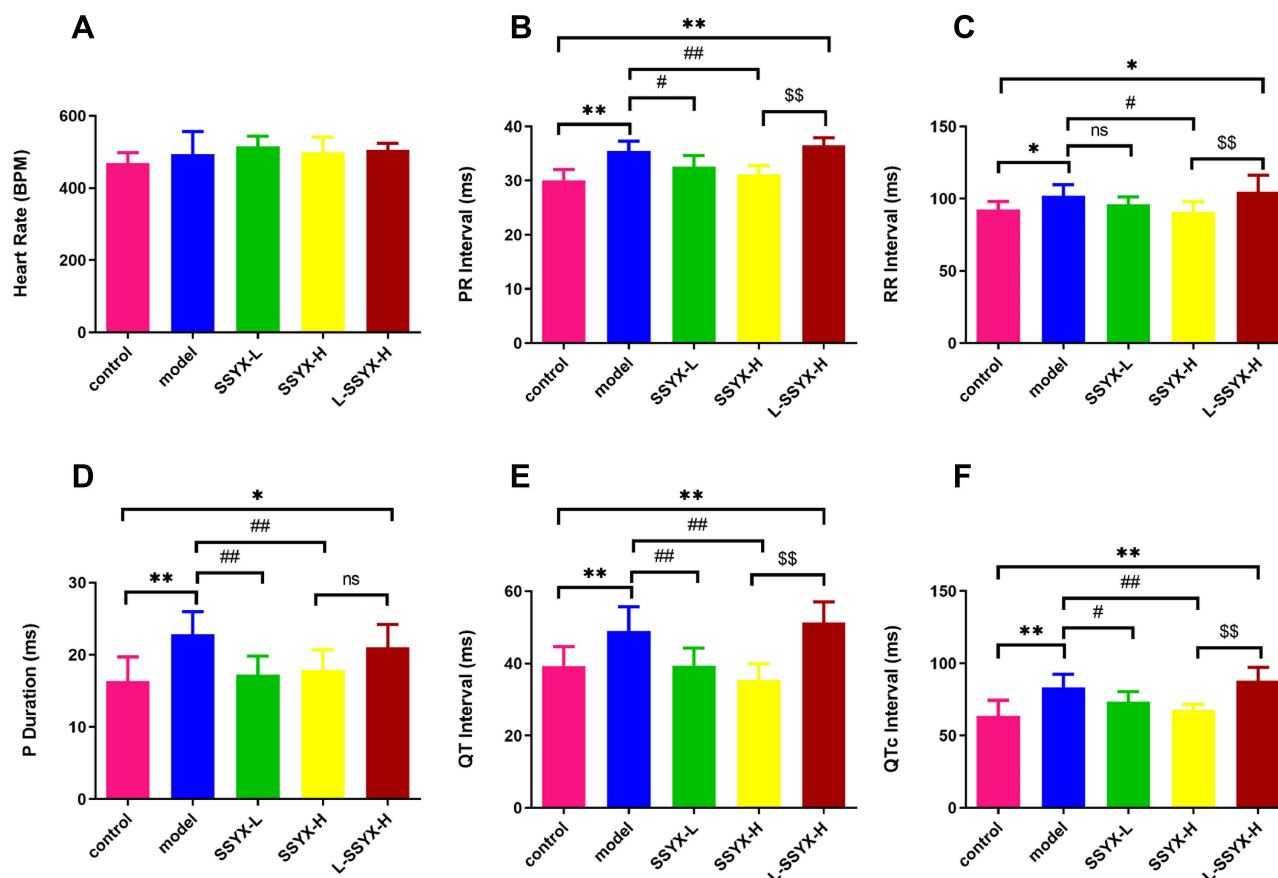


Figure 4 ECG parameters after intraperitoneal injection of isoproterenol in each group. (A) The heart rate, (B) PR interval, (C) RR interval, (D) P duration, (E) QT interval, and (F) QTc interval in each group. Values measured are presented as the mean \pm SD ($n = 6$). $^{**}P < 0.01$ vs control group. $^{*}P < 0.05$ vs control group. $^{###}P < 0.01$ vs model group. $^{#}P < 0.05$ vs model group. $^{$$}P < 0.01$ vs SSYX-H group. $^{*}P < 0.05$ vs SSYX-H group. **Abbreviations:** n.s., no statistical significance.

and disorganized myofibrillar arrangement. Compared with the model group, inflammatory cell infiltration and cardiomyocyte swelling were lower in the SSYX-L group and SSYX-H group.

In **Figure 8B**, Masson staining shows that collagen fibers were deposited in the model group and the L-SSYX-H group. The SSYX-L group and the SSYX-H group showed reduced collagen deposition compared with the model group.

SSYX Improved Endothelium Dysfunction in db/db Mice

As shown in **Figure 9A–C**, Western blot results indicated that the protein expression levels of ZO-1, eNOS, and occludin were reduced in the model group and the L-SSYX-H group compared with the control group ($P < 0.05$ or $P < 0.01$). Compared with the model group, the protein expression levels of ZO-1, eNOS and occludin were upregulated in the SSYX-L group and the SSYX-H group ($P < 0.05$ or $P < 0.01$). As shown in **Figure 9D**, ET-1 mRNA expression was upregulated in the model group and the L-SSYX-H group compared with the control group ($P < 0.01$). Compared with the model group, ET-1 mRNA expression was reduced in the SSYX-L group and the SSYX-H group ($P < 0.01$). As shown in **Figure 9E**, the NO content was reduced in the model group and the L-SSYX-H group compared with the control group ($P < 0.05$). Compared with the model group, the NO content was upregulated in the SSYX-H group ($P < 0.01$). Next, we observed, as shown in **Figure 9F**, that the fluorescence densities of eNOS and CD31 in the model group and L-SSYX-H group were decreased when compared with those in the control group, while in the SSYX-L group and SSYX-H group, they were increased when compared with those in the model group.

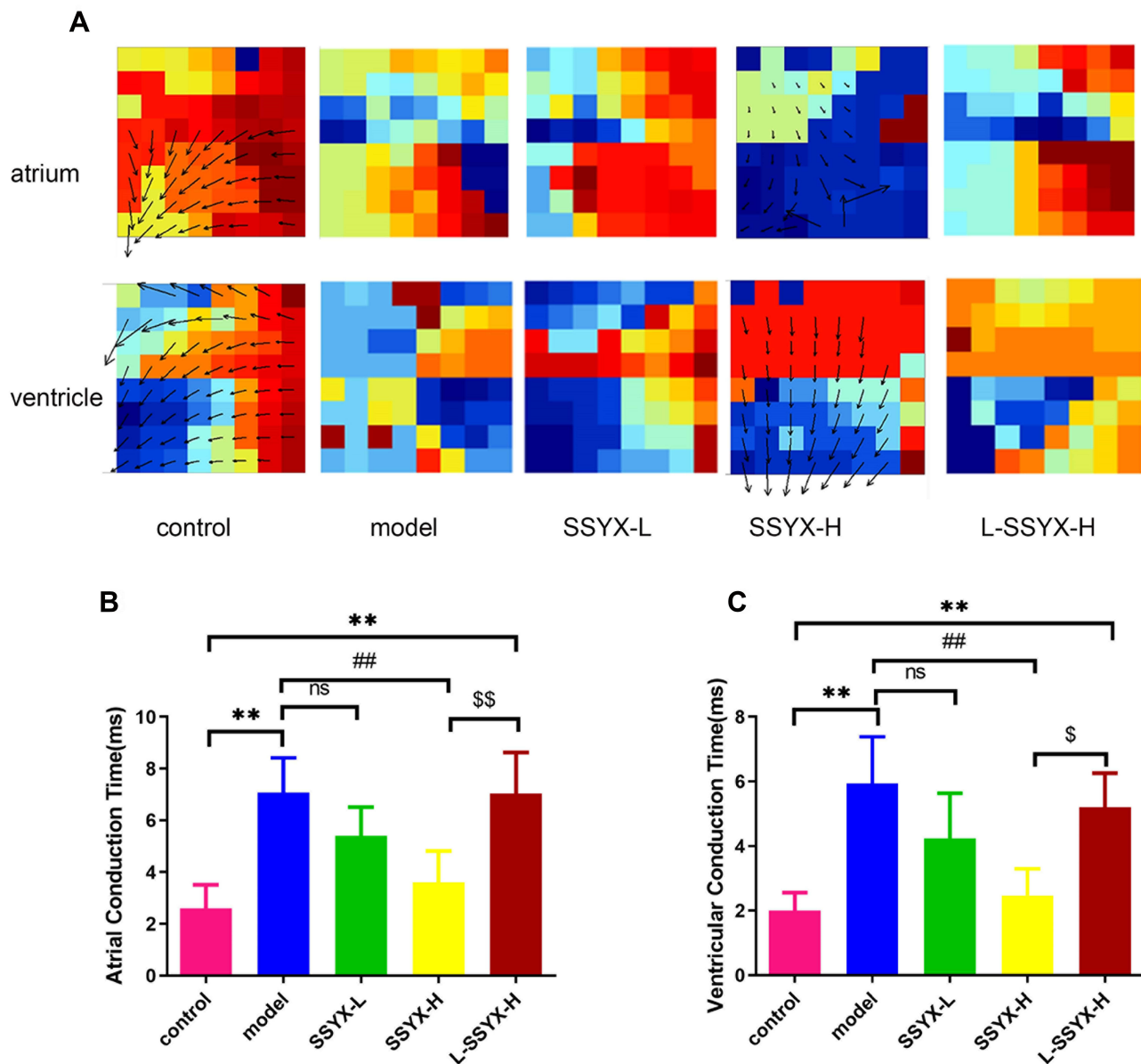


Figure 5 Conduction direction and time of isolated heart measured by electrical mapping. **(A)** Conduction direction of atrium and ventricle in each group. **(B)** Atrial conduction time and **(C)** ventricular conduction time in each group. Values measured are presented as the mean \pm SD ($n = 3$). ** $P < 0.01$ vs control group. ### $P < 0.01$ vs model group. \$\$\$ $P < 0.01$ vs SSYX-H group. \$ $P < 0.05$ vs SSYX-H group.

Abbreviations: n.s, no statistical significance.

SSYX Reduced Inflammatory Cytokine Secretion and Macrophage Polarization

As shown in Figure 10A–C, the protein expression levels of ICAM-1, VCAM-1, and MCP-1 were higher in the model group and the L-SSYX-H group compared with those in the control group ($P < 0.01$). Compared with the model group, the protein expression levels of ICAM-1, VCAM-1, and MCP-1 were decreased in the SSYX-L group and the SSYX-H group ($P < 0.05$ or $P < 0.01$). As shown in Figure 10D–H, MCP-1, IL-1 β , TNF- α , CCR-2, and IL-6 mRNA expression levels were upregulated in the model group and the L-SSYX-H group compared with those in the control group ($P < 0.05$ or $P < 0.01$). Compared with the model group, MCP-1, IL-1 β , TNF- α , CCR-2, and IL-6 mRNA expression levels were reduced in the SSYX-H group ($P < 0.05$ or $P < 0.01$). Next, we observed, as shown in Figure 10I, that the fluorescence densities of F4/80 and iNOS in the model group and the L-SSYX-H group were increased when compared with those in

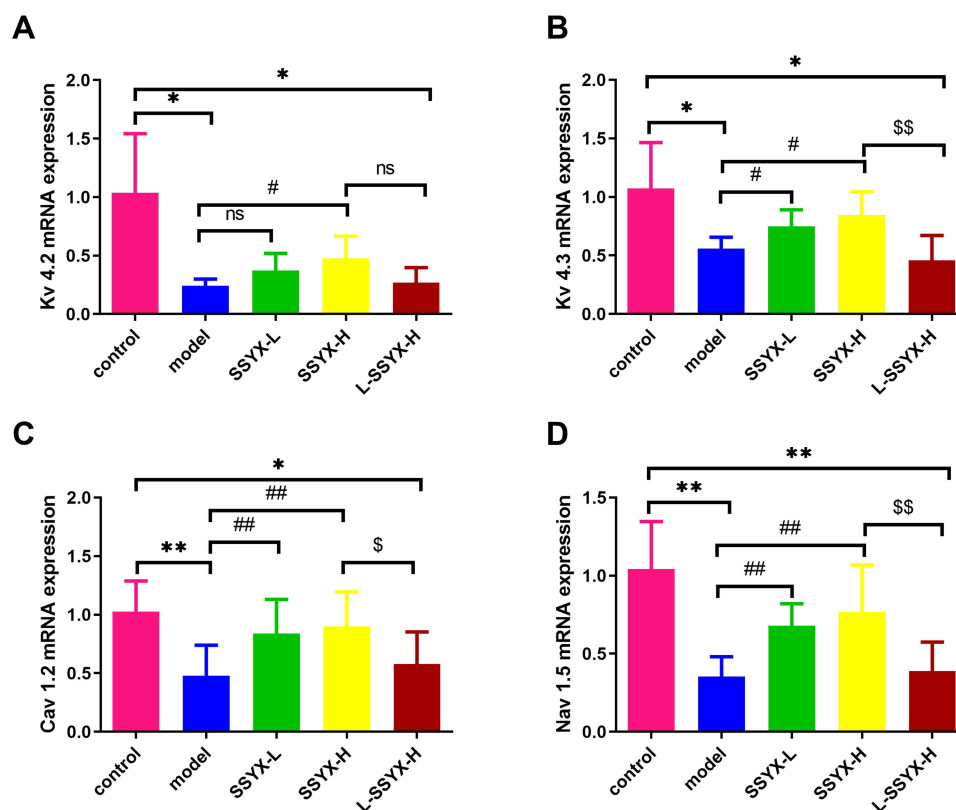


Figure 6 Effects of SSYX on the mRNA expression of Kv 4.2, Kv 4.3, Cav 1.2, and Nav 1.5. (A) Kv 4.2, (B) Kv 4.3, (C) Cav 1.2, and (D) Nav 1.5 mRNA expression levels were normalized to the arithmetic mean of GAPDH and analyzed using the threshold cycle (C_T) relative quantification method. The mRNA expression levels were quantified using the $2^{-\Delta\Delta C_T}$ method for comparison. Values measured are presented as the mean \pm SD ($n = 3$). ** $P < 0.01$ vs control group. * $P < 0.05$ vs control group. ### $P < 0.01$ vs model group. # $P < 0.05$ vs model group. \$\$\$ $P < 0.01$ vs SSYX-H group. \$ $P < 0.05$ vs SSYX-H group.

Abbreviations: n.s., no statistical significance.

the control group, while in the SSYX-L group and SSYX-H group, they were decreased when compared with those in the model group.

Discussion

The present study investigated the effect of SSYX on the arrhythmia susceptibility of db/db mice. In this study, we found that SSYX reduced arrhythmia susceptibility and improved abnormal ECG parameters in db/db mice. Electrical mapping showed that SSYX restored irregular cardiac conduction direction and shortened conduction time in db/db mice. We also observed that SSYX improved the gap junction structure of cardiomyocytes and decreased the deposition of collagen fibers in cardiac tissues of db/db mice. Furthermore, we found that SSYX decreased inflammatory cell infiltration in cardiac tissues and inhibited the secretion of inflammatory cytokines and macrophage polarization. We further confirmed the endothelial protective effect of SSYX on db/db mice, which contributed to its effects of inhibiting the inflammatory response and decreasing arrhythmia susceptibility.

The db/db mouse is a common model of diabetes because it has leptin receptor deficiency. This study showed that after stimulation with isoproterenol, db/db mice developed sinus node dysfunction, which triggered arrhythmia.²⁷ Another study demonstrated that db/db mice exhibited increased susceptibility to atrial fibrillation, which is associated with electrical and structural remodeling of the atria.²⁸ Our study showed that db/db mice were more likely to develop arrhythmia after intraperitoneal injection of isoproterenol. SSYX significantly reduced the arrhythmia susceptibility and shortened the PR interval, RR interval, P duration, QT interval, and QTc interval in db/db mice. Electrical mapping showed that SSYX restored the atrial and ventricular irregular conduction direction and shortened the conduction time in db/db mice. We also observed that SSYX increased the mRNA expressions of Kv 4.2, Kv 4.3, Cav 1.2, and Nav 1.5.

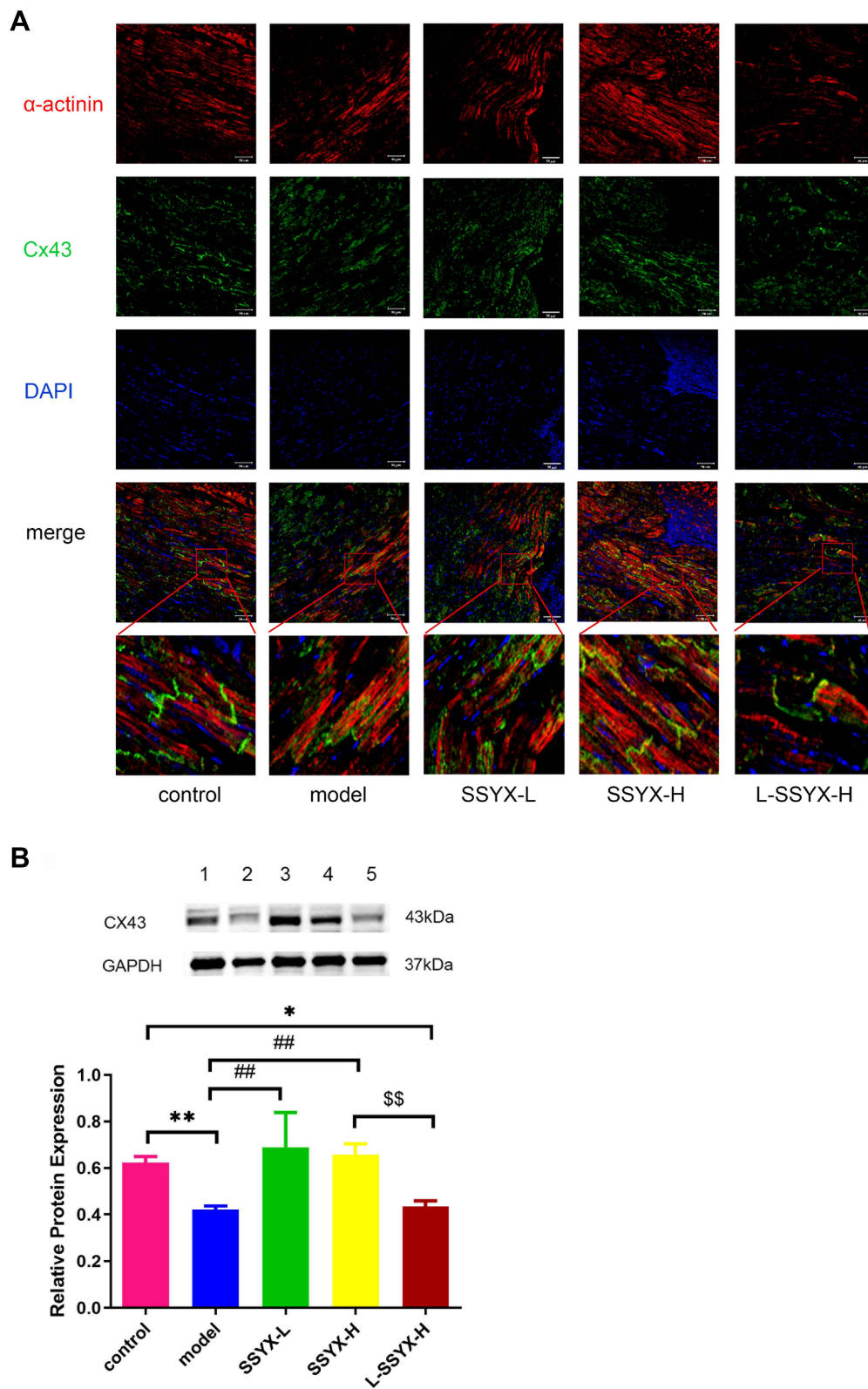


Figure 7 Effects of SSYX on the gap junction of myocardial cells and the protein expression of Cx43. **(A)** Representative images of immunofluorescence double staining for each group, α -actinin, Cx43, and DAPI were marked in red, green, and blue respectively (200 \times). **(B)** The protein expression of Cx43. Values measured are presented as the mean \pm SD (n = 3). ** P < 0.01 vs control group. * P < 0.05 vs control group. ### P < 0.01 vs model group. \$\$ P < 0.01 vs SSYX-H group. **Note:** 1: control, 2: model, 3: SSYX-L, 4: SSYX-H, 5: L-SSYX-H.

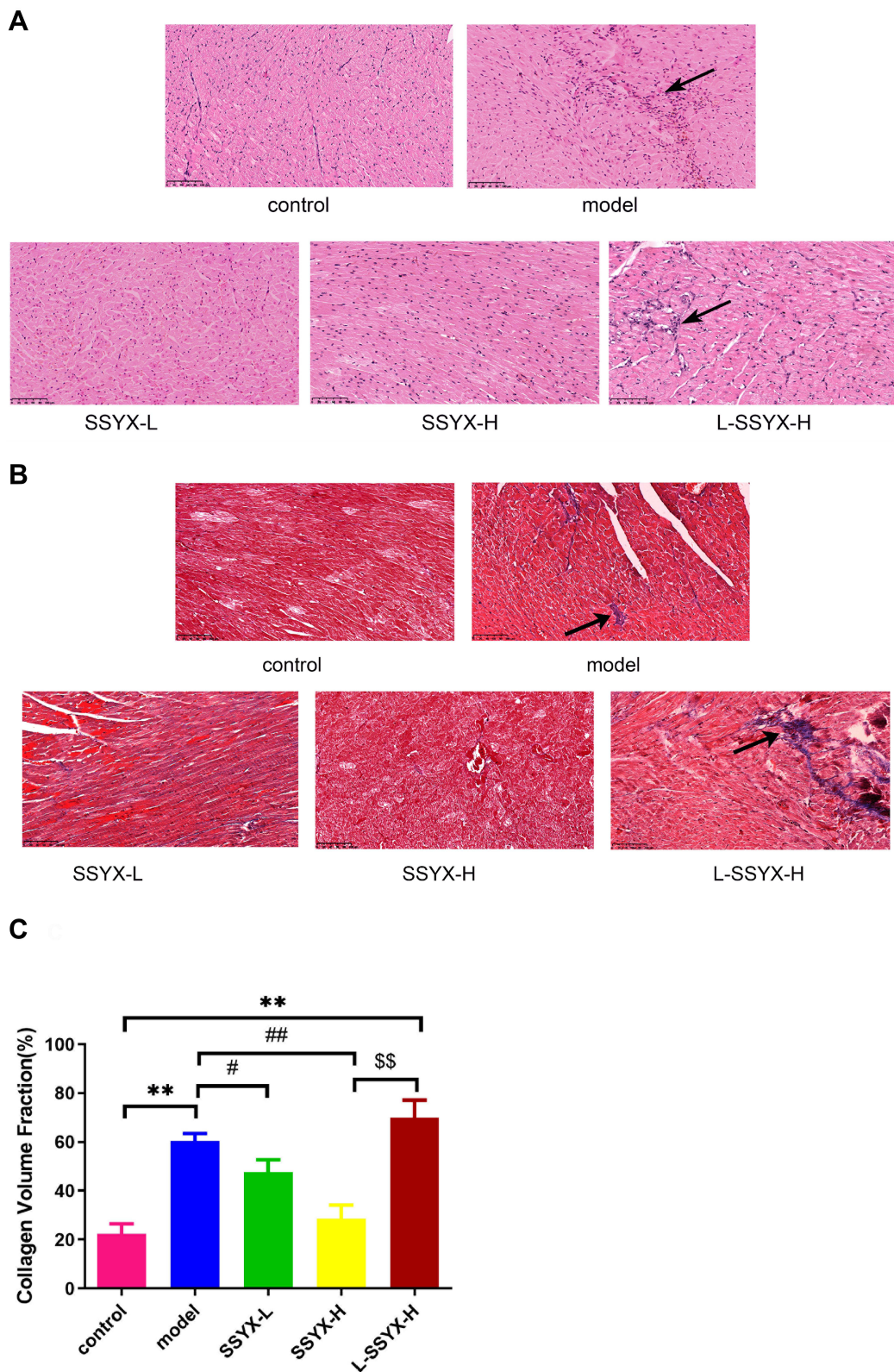


Figure 8 Effects of SSYX on histopathological changes of the heart observed by HE and Masson staining (200 ×). **(A)** Representative images of HE staining for each group. **(B)** Representative images of Masson staining for each group. **(C)** The myocardial collagen volume fraction of Masson staining. Values measured are presented as the mean ± SD (n = 3). ***P* < 0.01 vs control group. ##*P* < 0.01 vs model group. #*P* < 0.05 vs model group. \$\$*P* < 0.01 vs SSYX-H group.

Further pathological detection revealed that SSYX reduced cardiac collagen fiber deposition in db/db mice, which may be one of the mechanisms through which SSYX improves cardiac conduction and reduces arrhythmia susceptibility.

Previous research reported myocardial microcirculation dysfunction in organic heart diseases, and arrhythmia was often one of the concomitant clinical features.²⁹ Microcirculation dysfunction can affect endothelial cell function and further promote inflammation. The experiment reported that SSYX could ameliorate myocardial microcirculation dysfunction in rabbits with chronic myocardial infarction and protect endothelial cell function.¹⁸ To verify whether SSYX reduced arrhythmia susceptibility in db/db mice by protecting endothelial cell function, we selected L-NAME as an endothelial cell protection inhibitor. L-NAME is a competitive inhibitor of nitric oxide synthase; thus, it blocks NO production. NO is an endothelial relaxing factor and plays an important role in protecting endothelial cells. Our results showed that the therapeutic effect of SSYX was blocked by L-NAME, which indicated that SSYX reduced arrhythmia susceptibility in db/db mice by protecting endothelial cell function.

To further assess the extent of endothelial injury in db/db mice, we detected related indices of endothelial cell function in cardiac tissues. Tight junctions are an important component of endothelial barriers. Occludin is one of the essential ingredients of tight junctions. ZO-1 is one of the binding partners of occludin, and previous findings clarified that ZO-1 establishes a link between occludin and the actin cytoskeleton.³⁰ It has been reported that inflammatory diseases, such as diabetes, are associated with tight junction disruption and alterations in the regulation of occludin.³¹ Our study results showed that SSYX promoted the protein expression of ZO-1 and occludin in db/db mice, which supported the above findings and reflected impaired endothelial barrier function in db/db mice. ENOS can oxidize the terminal guanidine nitrogen atom of L-arginine to NO, and NO is an endothelial-derived relaxation factor.³² ET-1 is known as a

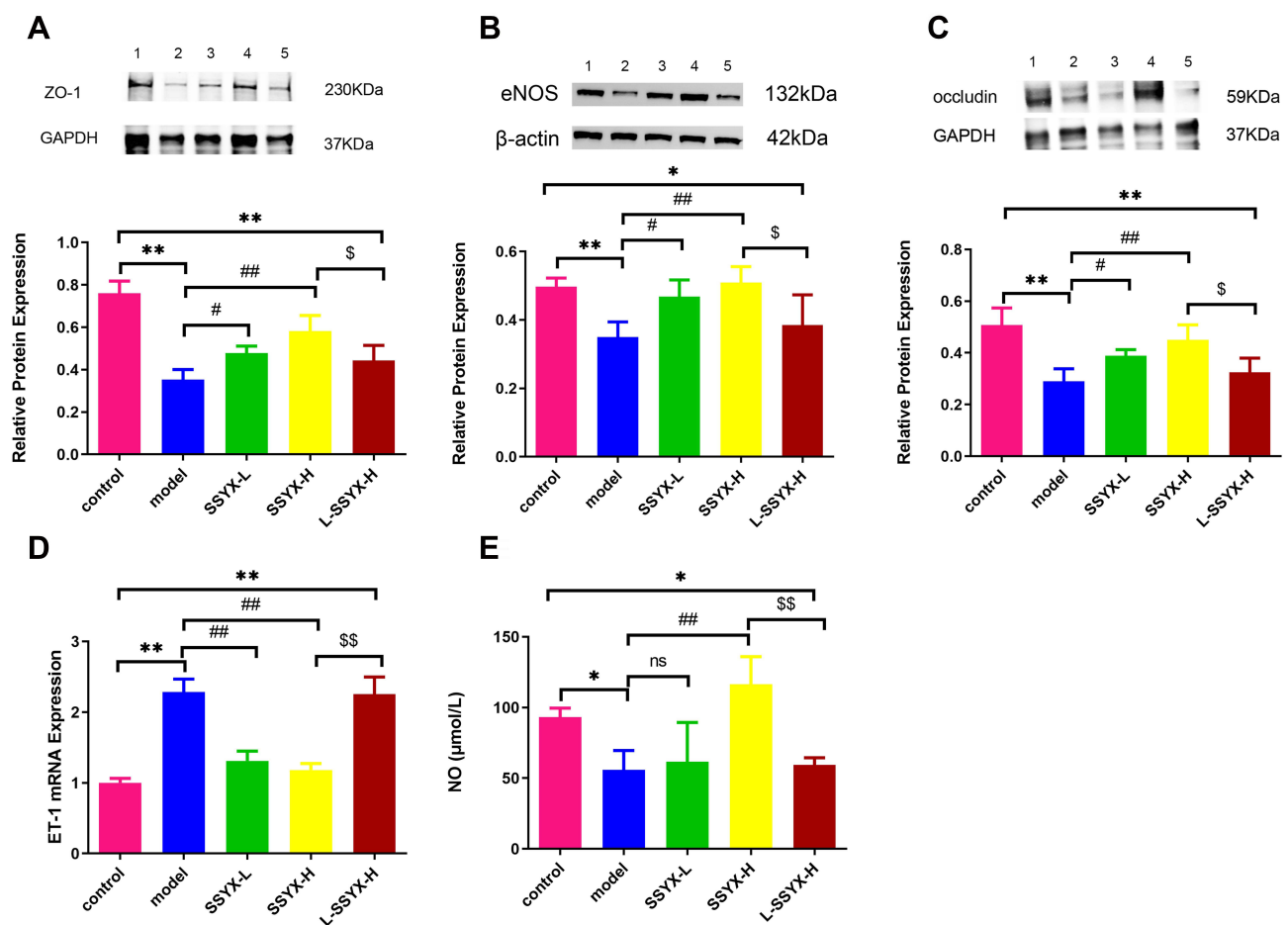


Figure 9 Continued.

F

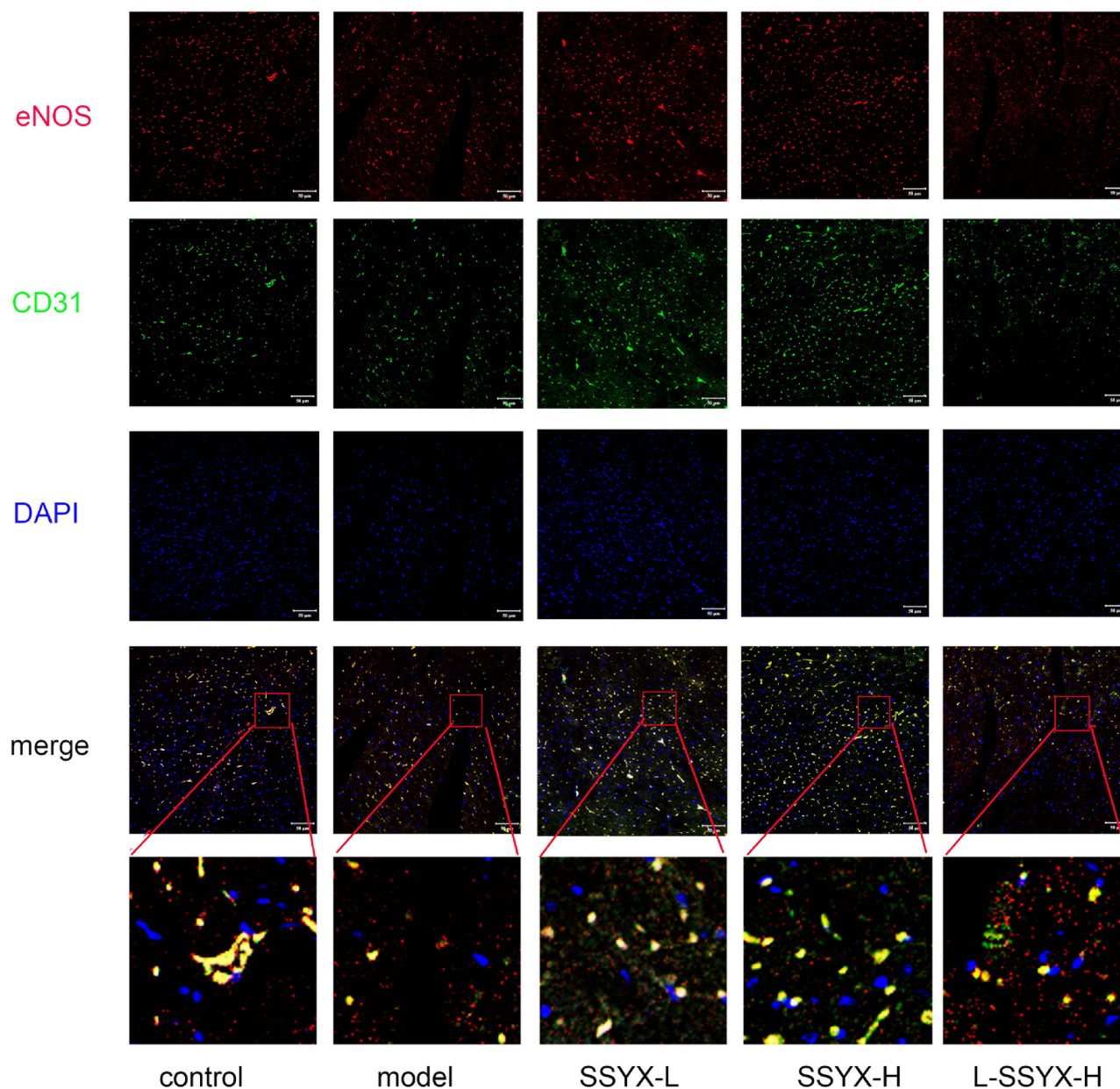


Figure 9 Effects of SSSYX on the protein expression of ZO-1, eNOS, occludin, the mRNA expression of ET-1, NO content, and the expression of CD31 and eNOS observed by immunofluorescence double staining in the heart tissue. The protein expression of (A) ZO-1, (B) eNOS, and (C) occludin in each group. (D) The ET-1 mRNA expression in each group. (E) The NO content in each group. (F) Representative images of immunofluorescence double staining for each group. ENOS, CD31, and DAPI were marked in red, green, and blue respectively. The overlap parts of CD31 and eNOS were marked in yellow (200 \times). Values measured are presented as the mean \pm SD (n = 3). ** $P < 0.01$ vs control group. * $P < 0.05$ vs control group. ### $P < 0.01$ vs model group. # $P < 0.05$ vs model group. \$\$ $P < 0.01$ vs SSSYX-H group. \$ $P < 0.05$ vs SSSYX-H group. **Note:** 1: control, 2: model, 3: SSSYX-L, 4: SSSYX-H, 5: L-SSYX-H.

potent vasoconstrictor that can stimulate leukocyte adhesion and recruitment. Our study found that SSSYX improved the protein expression of eNOS and the NO level in cardiac tissue and decreased ET-1 mRNA expression in db/db mice. This finding demonstrated that SSSYX restored the balance between endothelial-derived vasodilators and vasoconstrictors in db/db mice to protect endothelial cell function.

Endothelium dysfunction is a critical event in vascular inflammation. It is partially characterized by increased surface expression of adhesion molecules.³³ In our study, the protein expression of ICAM-1 and VCAM-1 increased in db/db cardiac tissue, and SSYX reduced their expression. Through pathological examination of the heart, we found inflammatory cell infiltration in the hearts of db/db mice. Activation of macrophages plays an important role in inflammation.³⁴ M1 macrophages produce proinflammatory cytokines, such as iNOS, TNF- α , MCP-1, and IL-1 β .³⁵ Our study results showed that SSYX decreased the protein expression of MCP-1 and the mRNA expression of TNF- α , IL-1 β , IL-6, MCP-1, and CCR-2. Immunofluorescence showed that SSYX reduced the fluorescence density of F4/80 and iNOS in the cardiac tissue of db/db mice. Resident macrophages can promote cardiac electrical conduction by forming gap junctions with cardiomyocytes.¹¹ Previous studies have shown that macrophage polarization can affect the gap junction structure of cardiomyocytes, resulting in arrhythmia.¹² Cx43 is a major component of the gap junction of cardiomyocytes. It can facilitate low resistance communication and rapid action potential transmission between adjacent cardiac cells.³⁶ α -Actinin is the structural protein of sarcomeres, which can stabilize electrical signals between cardiomyocytes and promote the synchronous contraction of cardiomyocytes.³⁷ The expression of α -actinin and Cx43 in cardiac tissue can reflect changes in the structural characteristics of cardiomyocytes. In our study, SSYX increased the protein expression of Cx43 and restored the structural position between Cx43 and α -actinin in db/db mice, which might be one of the reasons for its antiarrhythmic effect.

Conclusion

This study found that SSYX reduced arrhythmia susceptibility and improved electrophysiological abnormalities in db/db mice. Meanwhile, SSYX improved the cardiac tissue inflammatory response and collagen fiber deposition. Further analysis revealed that SSYX inhibited inflammatory factor release and macrophage polarization, and SSYX also improved endothelial cell function. Simultaneously, SSYX restored the structure between cardiomyocytes and gap junctions. These effects of SSYX were offset by L-NAME. Collectively, these results indicate that the effect of SSYX is exerted by protecting the function of endothelial cells.

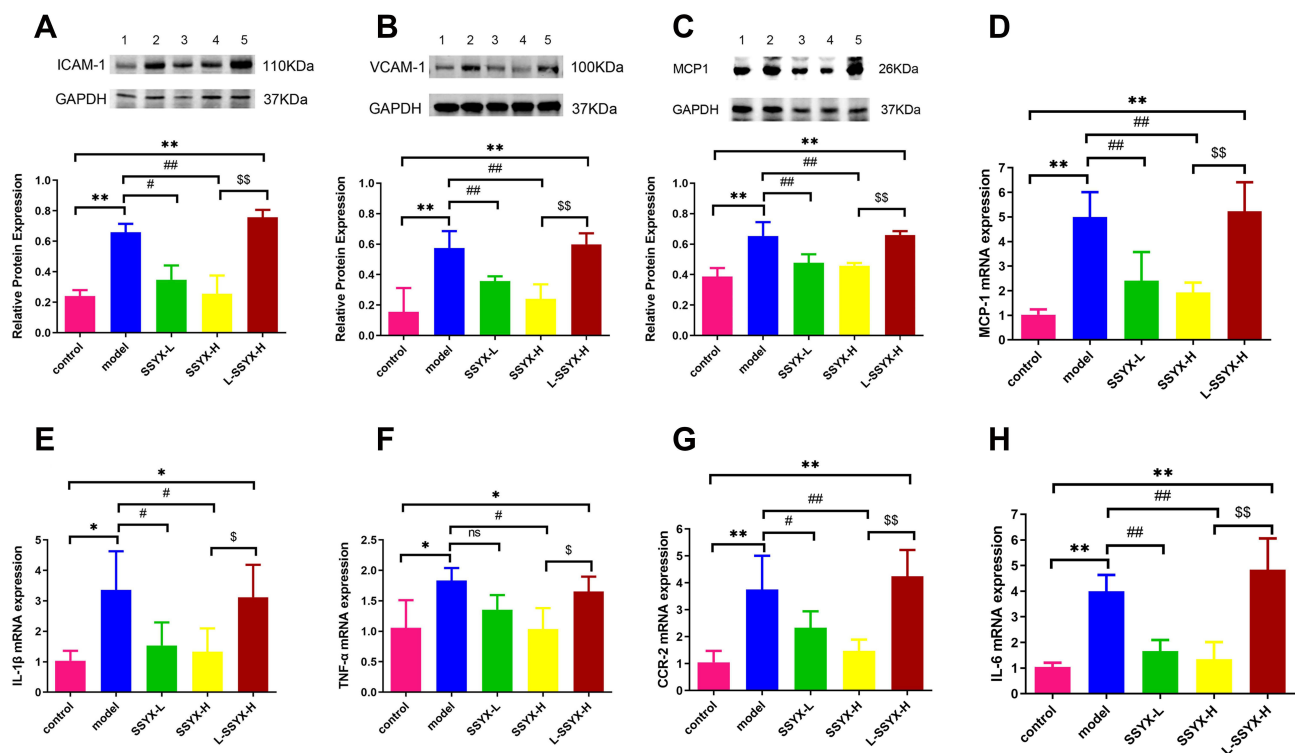


Figure 10 Continued.

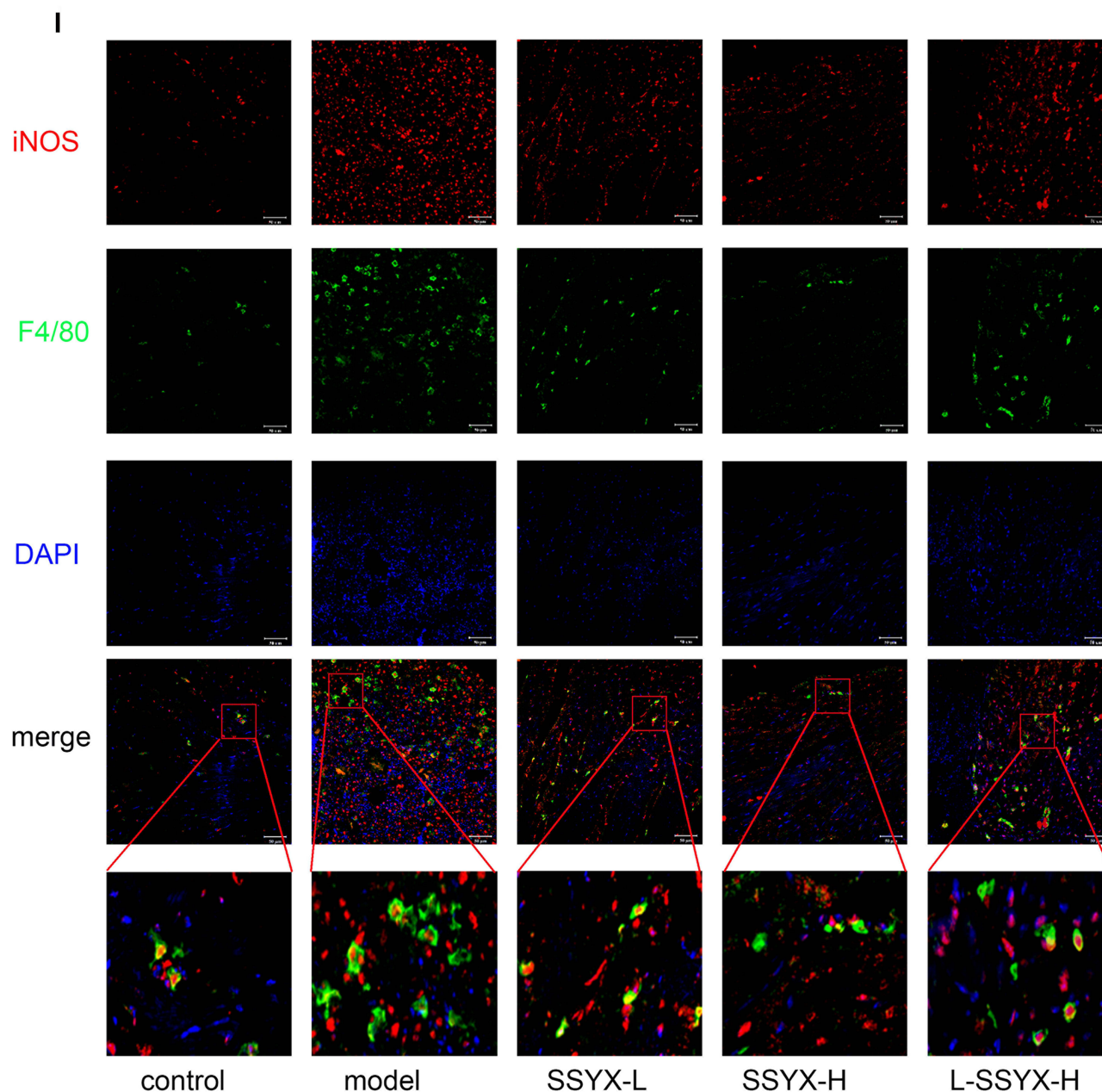


Figure 10 Effects of SSYX on the protein expression of ICAM-1, VCAM-1, MCP-1, the mRNA expression of MCP-1, IL-1 β , TNF- α , CCR-2, IL-6, and the expression of iNOS and F4/80 observed by immunofluorescence double staining in the heart tissue. The protein expression of (A) ICAM-1, (B) VCAM-1, and (C) MCP-1 in each group. The mRNA expression of (D) MCP-1, (E) IL-1 β , (F) TNF- α , (G) CCR-2, (H) IL-6 in each group. (I) Representative images of immunofluorescence double staining for each group. iNOS, F4/80, and DAPI were marked in red, green, and blue respectively (200 \times). Values measured are presented as the mean \pm SD (n = 3). ** P < 0.01 vs control group. * P < 0.05 vs control group. ### P < 0.01 vs model group. # P < 0.05 vs model group. \$ P < 0.01 vs SSYX-H group. $\text{\$}P$ < 0.05 vs SSYX-H group.

Note: 1: control, 2: model, 3: SSYX-L, 4: SSYX-H, 5: L-SSYX-H.

Acknowledgments

This work was supported by the National Key Research Program “Research on the Modernization of Traditional Chinese Medicine” key special funded project (grant number 2017YFC1700500) and the Hebei Provincial Administration of Traditional Chinese Medicine Scientific Research Program Project (grant number 2022216).

Disclosure

The authors report no conflicts of interest in this work.

References

1. Zeng Z, Zhuang Z, He Y, et al. Efficacy and safety of Shen-Song-Yang-Xin capsule for treating arrhythmia in the elderly patients with coronary heart disease: protocol for a systematic review and meta-analysis. *Medicine*. 2018;97(51):e13599. doi:10.1097/MD.00000000000013599
2. Driessen HE, van Veen TAB, Boink GJJ. Emerging molecular therapies targeting myocardial infarction-related arrhythmias. *Europace*. 2017;19(4):518–528. doi:10.1093/europace/euw198
3. Roubille F, Tardif JC. New therapeutic targets in cardiology: heart failure and arrhythmia: HCN channels. *Circulation*. 2013;127(19):1986–1996. doi:10.1161/CIRCULATIONAHA.112.000145
4. Yang KC, Nerbonne JM. Mechanisms contributing to myocardial potassium channel diversity, regulation and remodeling. *Trends Cardiovasc Med*. 2016;26(3):209–218. doi:10.1016/j.tcm.2015.07.002
5. Burchfield JS, Xie M, Hill JA. Pathological ventricular remodeling: mechanisms: part 1 of 2. *Circulation*. 2013;128(4):388–400. doi:10.1161/CIRCULATIONAHA.113.001878
6. Abrams D, Schilling R. Mechanism and mapping of atrial arrhythmia in the modified Fontan circulation. *Heart Rhythm*. 2005;2(10):1138–1144. doi:10.1016/j.hrthm.2005.07.009
7. Corban MT, Taya T, Ahmad A, et al. Atrial fibrillation and endothelial dysfunction: a potential link? *Mayo Clin Proc*. 2021;96(6):1609–1621. doi:10.1016/j.mayocp.2020.11.005
8. Corban MT, Lerman LO, Lerman A. Endothelial dysfunction. *Arterioscler Thromb Vasc Biol*. 2019;39(7):1272–1274. doi:10.1161/ATVBAHA.119.312836
9. Grune J, Yamazoe M, Nahrendorf M. Electroimmunology and cardiac arrhythmia. *Nat Rev Cardiol*. 2021;18(8):547–564. doi:10.1038/s41569-021-00520-9
10. Nicolás-ávila JA, Lechuga-Vieco AV, Esteban-Martínez L, et al. A network of macrophages supports mitochondrial homeostasis in the heart. *Cell*. 2020;183(1):94–109.e23. doi:10.1016/j.cell.2020.08.031
11. Hulsmans M, Clauss S, Xiao L, et al. Macrophages facilitate electrical conduction in the heart. *Cell*. 2017;169(3):510–522.e20. doi:10.1016/j.cell.2017.03.050
12. Fei YD, Wang Q, Hou JW, et al. Macrophages facilitate post myocardial infarction arrhythmias: roles of gap junction and KCa3.1. *Theranostics*. 2019;9(22):6396–6411. doi:10.7150/thno.34801
13. Jungen C, Scherschel K, Flenner F, et al. Increased arrhythmia susceptibility in type 2 diabetic mice related to dysregulation of ventricular sympathetic innervation. *Am J Physiol Heart Circ Physiol*. 2019;317(6):H1328–H1341. doi:10.1152/ajpheart.00249.2019
14. Staerk L, Sherer JA, Ko D, et al. Atrial fibrillation: epidemiology, pathophysiology, and clinical outcomes. *Circ Res*. 2017;120(9):1501–1517. doi:10.1161/CIRCRESAHA.117.309732
15. Russo S, Kwiatkowski M, Govorukhina N, et al. Meta-inflammation and metabolic reprogramming of macrophages in diabetes and obesity: the importance of metabolites. *Front Immunol*. 2021;12(12):746151. doi:10.3389/fimmu.2021.746151
16. Rendra E, Riabov V, Mossel DM, et al. Reactive oxygen species (ROS) in macrophage activation and function in diabetes. *Immunobiology*. 2019;224(2):242–253. doi:10.1016/j.imbio.2018.11.010
17. Shi Y, Vanhoutte PM. Macro- and microvascular endothelial dysfunction in diabetes. *J Diabetes*. 2017;9(5):434–449. doi:10.1111/1753-0407.12521
18. Jiang C, Wang X, Dang S, et al. Chinese Medicine Shensong Yangxin capsule () ameliorates myocardial microcirculation dysfunction in rabbits with chronic myocardial infarction. *Chin J Integr Med*. 2021;27(1):24–30. doi:10.1007/s11655-018-2578-1
19. Dang S, Huang CX, Wang X, et al. Shensong Yangxin (SSYX) ameliorates disordered excitation transmission by suppressing cardiac collagen hyperplasia in rabbits with chronic myocardial infarction. *J Huazhong Univ Sci Technol Med Sci*. 2016;36(2):162–167. doi:10.1007/s11596-016-1560-4
20. Yang HJ, Kong B, Shuai W, et al. Shensong Yangxin protects against metabolic syndrome-induced ventricular arrhythmias by inhibiting electrical remodeling. *Front Pharmacol*. 2020;11:993. doi:10.3389/fphar.2020.00993
21. Shen DF, Wu QQ, Ni J, et al. Shensongyangxin protects against pressure overload-induced cardiac hypertrophy. *Mol Med Rep*. 2016;13(1):980–988. doi:10.3892/mmr.2015.4598
22. Shen N, Li X, Zhou T, et al. Shensong Yangxin capsule prevents diabetic myocardial fibrosis by inhibiting TGF- β 1/Smad signaling. *J Ethnopharmacol*. 2014;157:161–170. doi:10.1016/j.jep.2014.09.035
23. Ma J, Yin C, Ma S, et al. Shensong Yangxin capsule reduces atrial fibrillation susceptibility by inhibiting atrial fibrosis in rats with post-myocardial infarction heart failure. *Drug Des Devel Ther*. 2018;12:3407–3418. doi:10.2147/DDDT.S182834
24. Zhao HY, Zhang SD, Zhang K, et al. Effect of Shensong Yangxin on the progression of paroxysmal atrial fibrillation is correlated with regulation of autonomic nerve activity. *Chin Med J*. 2017;130(2):171–178. doi:10.4103/0366-6999.197997
25. Li N, Ma KJ, Wu XF, et al. Effects of Chinese herbs on multiple ion channels in isolated ventricular myocytes. *Chin Med J*. 2007;120(12):1068–1074. doi:10.1097/00029330-200706020-00008
26. Yang HJ, Kong B, Shuai W, et al. Shensong Yangxin attenuates metabolic syndrome-induced atrial fibrillation via inhibition of ferroportin-mediated intracellular iron overload. *Phytomedicine*. 2022;101:154086. doi:10.1016/j.phymed.2022.154086
27. Lubberding AF, Pereira L, Xue J, et al. Aberrant sinus node firing during β -adrenergic stimulation leads to cardiac arrhythmias in diabetic mice. *Acta Physiol*. 2020;229(1):e13444. doi:10.1111/apha.13444
28. Bohne LJ, Jansen HJ, Daniel I, et al. Electrical and structural remodeling contribute to atrial fibrillation in type 2 diabetic db/db mice. *Heart Rhythm*. 2021;18(1):118–129. doi:10.1016/j.hrthm.2020.08.019
29. Selthofer-Relatic K, Mihalj M, Kibel A, et al. Coronary microcirculatory dysfunction in human cardiomyopathies: a pathologic and pathophysiological review. *Cardiol Rev*. 2017;25(4):165–178. doi:10.1097/CRD.0000000000000140
30. Fanning AS, Jameson BJ, Jesaitis LA, et al. The tight junction protein ZO-1 establishes a link between the transmembrane protein occludin and the actin cytoskeleton. *J Biol Chem*. 1998;273(45):29745–29753. doi:10.1074/jbc.273.45.29745
31. Feldman GJ, Mullin JM, Ryan MP. Occludin: structure, function and regulation. *Adv Drug Deliv Rev*. 2005;57(6):883–917. doi:10.1016/j.addr.2005.01.009
32. Couto GK, Britto LR, Mill JG, et al. Enhanced nitric oxide bioavailability in coronary arteries prevents the onset of heart failure in rats with myocardial infarction. *J Mol Cell Cardiol*. 2015;86:110–120. doi:10.1016/j.yjmcc.2015.07.017

33. Regal-McDonald K, Somarathna M, Lee T, et al. Assessment of ICAM-1 N-glycoforms in mouse and human models of endothelial dysfunction. *PLoS One*. 2020;15(3):e0230358. doi:10.1371/journal.pone.0230358
34. Liu J, Zhang Y, Sheng H, et al. Hyperoside suppresses renal inflammation by regulating macrophage polarization in mice with type 2 diabetes mellitus. *Front Immunol*. 2021;12:733808. doi:10.3389/fimmu.2021.733808
35. Lim AK, Tesch GH. Inflammation in diabetic nephropathy. *Mediators Inflamm*. 2012;2012:146154. doi:10.1155/2012/146154
36. Epifantseva I, Shaw RM. Intracellular trafficking pathways of Cx43 gap junction channels. *Biochim Biophys Acta Biomembr*. 2018;1860(1):40–47. doi:10.1016/j.bbamem.2017.05.018
37. Sjöblom B, Salmazo A, Djinović-Carugo K. Alpha-actinin structure and regulation. *Cell Mol Life Sci*. 2008;65(17):2688–2701. doi:10.1007/s00018-008-8080-8

Drug Design, Development and Therapy

Dovepress

Publish your work in this journal

Drug Design, Development and Therapy is an international, peer-reviewed open-access journal that spans the spectrum of drug design and development through to clinical applications. Clinical outcomes, patient safety, and programs for the development and effective, safe, and sustained use of medicines are a feature of the journal, which has also been accepted for indexing on PubMed Central. The manuscript management system is completely online and includes a very quick and fair peer-review system, which is all easy to use. Visit <http://www.dovepress.com/testimonials.php> to read real quotes from published authors.

Submit your manuscript here: <https://www.dovepress.com/drug-design-development-and-therapy-journal>